Dependence of the Rate Constants on the Treatment of Internal Rotation Modes: The Reaction OH + CH_3SH → CH_3S + H_2O as an Example

LAURA MASGRAU, ÀNGELS GONZÁLEZ–LAFONT, JOSÉ M. LLUCH
Departament de Química, Universitat Autònoma de Barcelona, 08193 Bellaterra (Barcelona), Spain

Received 24 June 2002; Accepted 14 August 2002

Abstract: The title reaction has been used as an example to test the importance of using a hindered rotor treatment instead of a harmonic oscillator model for calculating vibrational partition functions corresponding to low-frequency internal rotation modes. First, a normal-mode analysis according to the Ayala and Schlegel's algorithm has been used to identify the internal rotation modes of methanethiol and the transition state structure. Then, after calculation of the energy barrier for each internal rotation, the corresponding hindered rotor partition functions have been calculated following the CW scheme of Chuang and Truhlar. The results show that the anharmonic treatment produces a rather modest improvement of the rate constants at room temperature or below.

 J Comput Chem 24: 701–706, 2003

Key words: hindered rotor; internal rotation modes; rate constant calculations; vibrational partition functions; total torsion contribution

Introduction

Today, transition state theory[1–3] is the most extensively and successfully used procedure to calculate accurate values of gas-phase thermal reaction rate constants. According to canonical conventional transition state theory the rate constant for a bimolecular reaction is expressed in terms of partition functions as

$$k(T) = \kappa(T) V \frac{\sigma k_B T}{h} \frac{q^{\ddagger}(T)}{q_A(T) q_B(T)} e^{-(V^{\ddagger}/k_B T)} \quad (1)$$

where $\kappa(T)$ is the transmission factor that accounts for the quantum mechanical tunneling along the reaction coordinate, V is the volume, σ is the symmetry factor, $q^{\ddagger}$ is the conventional transition state partition function, $q_A(T)$ and $q_B(T)$ are the reactants partition function (excluding symmetry numbers for rotation in the calculation of all the partition functions), $V^{\ddagger}$ is the classical potential energy barrier, and k_B is the Boltzmann's constant.

The partition functions involve a summation of Boltzmann factors over the electronic–vibrational–rotational and translational energy levels. Applying the Born–Oppenheimer approximation and assuming a rigid rotor model, couplings between electronic, vibrational, and rotational energies are neglected in such a way that the overall partition functions may be expanded as a product of electronic, vibrational, rotational, and translational partition functions.

In this article we are concerned with the vibrational partition functions.[4] Assuming an independent normal-mode framework (i.e., no mode–mode coupling), the vibrational partition function of a molecule is separable as a product of the contributions corresponding to each individual normal mode. At the stationary points the potential energy along a single mode can be expanded in a series of powers of the associated normal coordinate with coefficients given by the second, third, fourth, and higher numerical directional derivatives of the potential energy along the normal-mode direction. If the vibrational energy levels E_i^m of the one-dimensional potential energy along the mode m can be determined in some way, the vibrational partition function for mode m can be calculated as

$$q_m = \sum_i e^{-(E_i^m/k_B T)} \quad (2)$$

If the terms of an order higher than 2 are neglected, the usual harmonic approximation, in which the energy levels and the partition functions are directly calculated from the harmonic vibrational frequencies, is obtained.

Correspondence to: A. González–Lafont; e-mail: angels@klingon.uab.es
Contract/grant sponsor: D6ESIC; contract/grant number PB98-0915

Sometimes the neglect of anharmonicity effects can be a major source of error in the evaluation of the vibrational partition functions. This is especially the case for low-frequency internal rotation modes, for which a hindered rotor treatment should be rather employed.[5–14] Treating these bond torsional modes in the right way is especially important at the transition state structures where the existence of several weak chemical bonds favors the appearance of such modes.

Recently, Ayala and Schlegel[15] have developed a procedure to identify internal rotation modes and the corresponding rotating groups during a normal mode vibrational analysis, making extensive use of the information embedded in the redundant internal coordinates.[16,17] More recently, Chuang and Truhlar[18,19] have presented a hindered rotor treatment for torsions in molecules with nonsymmetry-related multiple minima along the internal rotation coordinate, and several schemes to calculate the corresponding effective moments of inertia. Then, the purpose of this article is to utilize those methods to test the importance of using a hindered rotor treatment instead of a harmonic oscillator model for calculating vibrational partition functions corresponding to low-frequency internal rotation modes. We will intend to assess the sensitivity of the rate constants to the kind of treatment employed in a wide range of temperatures. To this aim, we have chosen as an illustrative example the reaction

$$OH + CH_3SH \rightarrow CH_3S + H_2O \qquad (3)$$

which is the major product channel of the reaction of methanethiol with OH radicals in the troposphere.[20–28] The reaction shown in eq. (3) occurs through a transition state structure that includes three bond torsional modes involving three respective classical energy barriers of clearly different size. This fact provides the opportunity to illustrate the different behavior of those modes as a function of their frequencies and their influence in the rate constant.

Method of Calculation

First, we present some technical details corresponding to the electronic structure calculations. Second, the nuclear motion treatment to identify the internal rotation modes and to evaluate the hindered rotor partition functions is outlined.

Electronic Structure Calculations

The electronic structure calculations have been carried out using the second-order Møller–Plesset perturbation theory (MP2)[29] based on restricted Hartree–Fock or unrestricted Hartree–Fock wave functions for closed-shell and open-shell systems, respectively, and with a full electron correlation treatment. A correlation-consistent polarized-valence triple zeta (cc-pVTZ)[30] basis set of Dunning with pure d and f functions has been employed. Full geometry optimization and direct location of stationary points have been done with Schlegel's gradient optimization algorithm,[31] using redundant internal coordinates.[16,17] The characterization of the different kinds of stationary points, minima, transition state structures, or second-order saddle points, has been performed by diagonalizing their Hessian matrices in mass-weighted Cartesian coordinates and looking for zero, one, or two negative eigenvalues, respectively. These diagonalizations also provide the corresponding vibrational harmonic frequencies. All the electronic calculations have been carried out with the GAUSSIAN 98 series of programs.[32]

Nuclear Motion Treatment

To identify the internal rotation modes at the reactants and the transition state structure, a normal-mode analysis has been performed with the POLYRATE 8.7 code[33] in the redundant internal coordinates[16] used in the GAUSSIAN 98 package. Previously, the corresponding Hessian matrices have been transformed from mass-weighted Cartesian coordinates to redundant internal coordinates. At each structure the internal rotations have been recognized following the algorithm developed by Ayala and Schlegel.[15] First, a cutoff value (in this case 96%) has been chosen to define the minimum amount of torsion that has to be present in a normal mode to be considered an internal rotation mode. For the ith normal mode, the magnitude of the dihedral components for each unique B—C bond

$$T(B-C, i) = \left(\sum_{(A,D)} L^2_{i(A,B,C,D)} \right)^{1/2} \qquad (4)$$

where the L_is are the dihedral components for mode i, has been tabulated. Then, the total torsion contribution present in normal mode i is obtained by calculating

$$\left(\sum_{B-C} T^2(B-C, i) \right)^{1/2}.$$

The bonds involved in internal rotation turn out to be the bonds that have the largest

$$\sum_i T(B-C, i)$$

when summed over the internal rotation modes. For each bond about which internal rotation occurs, the two rotating groups can be identified using the bonding information present in the set of internal coordinates. Then, according to Pitzer,[34–36] the corresponding effective moments of inertia are estimated from the moments of inertia of two unsymmetrical tops that rotate with respect to one another.

Finally, the hindered rotor partition functions (q^{HR}) corresponding to an identified internal rotation mode i have been calculated using the treatment developed by Chuang and Truhlar[19] for the case of a molecule with a single low-frequency torsion, with P approximately equally spread nonsymmetrically equivalent minima, each of symmetry σ_j, with $j = 1, \ldots, P$:

$$q^{HR} = q^{HO} \tanh \frac{q^{FR}}{q^{I}} \qquad (5)$$

where q^{HR} is interpolated between the harmonic partition function (q^{HO}) that includes contributions of the P nonsymmetrically equivalent minima found along the torsional coordinate, and the classical free rotor partition function (q^{FR}). In particular, we have used the so-called CW scheme,[19] which obtains the moment of inertia I_j from the Pitzer model,[34–36] obtains the energy barrier W_j for each internal rotation from electronic structure calculations, and estimates the vibrational harmonic frequencies (in wave numbers) for the internal rotation by means of

$$\bar{\nu}_j = \frac{1}{2\pi c}\left(\frac{W_j}{2I_j}\right)^{1/2} M \tag{6}$$

where c is the speed of light, and M is the total number of minima along the torsional coordinate in the range $0–2\pi$:

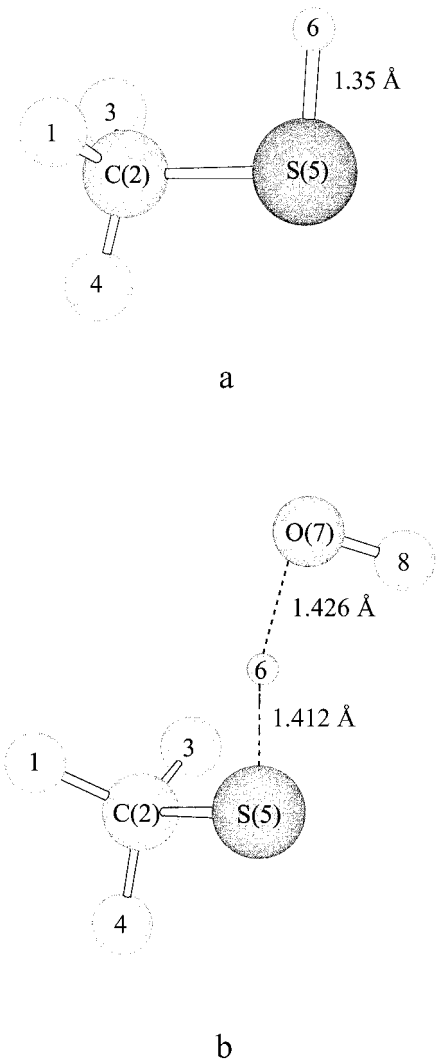

Figure 1. Methanethiol (a) and transition state structure (b) (dihedral angle O7H6S5C2 = 65.6°).

Table 1. Normal Mode Frequencies Derived from the Diagonalization of the Hessian, Dihedral Components and Total Torsion Contribution Present in the Three Internal Rotation Modes at the Transition State Structure.

Mode i	17	16	15
$\bar{\nu}$ (cm^{-1})	101.5	129.5	214.2
$T(2\text{-}5,\ i)$	91.9	69.4	37.7
$T(6\text{-}5,\ i)$	34.7	43.7	18.5
$T(7\text{-}6,\ i)$	17.8	50.7	88.2
$(\Sigma_{B-C} T^2(B-C, i))^{1/2}$	99.9	96.4	97.7

$$M = \sum_{j=1}^{P} \sigma_j \tag{7}$$

Then, q^{HO} in eq. (5) is calculated using the $\bar{\nu}_j$ values obtained through eq. (6), and q^I is given by the high-T limit of q^{HO}.

Results and Discussion

The structures of methanethiol and the transition state of the reaction corresponding to eq. (3) are shown in Figure 1. Comparing both structures it can be seen that at the transition state the hydrogen attached to the sulfur end of methanethiol has clearly weakened its bond with the sulfur, whereas it is already forming an incipient bond with the hydroxyl oxygen. Concurrently with this, the transition vector is almost entirely defined by the internal coordinates associated with both bonds.

After the normal-mode analysis, according to the Ayala and Schlegel's algorithm[15] only 1 of the 12 normal modes of methanethiol is identified as an internal rotation mode, involving a total torsion contribution of 100%. As expected, it corresponds to a pure internal rotation of the methyl group around the C2—S5 bond. The scenario is somewhat more complicated at the transition state structure, whose results are shown in Table 1. In this case, 3 of the 17 normal modes orthogonal to the transition vector have a total torsion contribution higher than the cutoff previously chosen. Mode 17 is an almost pure internal rotation mode consisting basically of the internal rotation of methyl group around the C2—S5 bond, although here with some contributions of the OH rotation around the H6—S5 breaking bond and the rotation of the hydroxyl hydrogen around the O7—H6 forming bond. In turn, mode 15 essentially corresponds to the rotation of the hydroxyl hydrogen around the O7—H6 bond. In contrast, mode 16 involves important dihedral components for the three bonds, C2—S5, H6—S5, and O7—H6.

For all those vibrational modes characterized as internal rotation modes the hindered rotor partition functions have to be calculated to substitute the corresponding harmonic partition functions. To this aim, according to the CW scheme,[19] we have first determined the energy barrier for each internal rotation:

1. Internal rotation mode at the methanethiol. As a function of the dihedral angle H1C2S5H6 (methyl rotation) we have built up an energy profile, the rest of the coordinates being optimized at each point. Because, as expected, three symmetrically equivalent minima appear, $P = 1$ and $\sigma = 3$. Then, from the higher energy points of the energy profile a first-order saddle point for the rotation has been directly located using the Schlegel's algorithm.[31]
2. Mode 17 at the transition state structure. This mode again corresponds to the methyl rotation according to the dihedral angle H1C2S5H6. The problem is that the rotation has to be done at a structure that is already a first-order saddle point and it does not have to imply any displacement in the direction of the transition vector. One way to do this is by constructing an energy profile as a function of the dihedral angle H1C2S5H6, keeping frozen the remainder of the coordinates. However, in doing this rigid approach an important hysteresis appears, provoking that the appropriate symmetry of the energy profile does not hold (i.e., the three minima along the path are not equivalent).[37–39] As an alternative, the energy profile has been rebuilt now relaxing the rest of the coordinates except the distances H6—S5 and O7—H6. Three symmetrically equivalent minima appear, which implies $P = 1$ and $\sigma = 3$. Then, from the higher energy points of this energy profile a second-order saddle point for the rotation has been directly located using the Schlegel's algorithm[31] but maintaining again those two distances frozen.
3. Mode 16 at the transition state structure. As above, rigid rotation varying the dihedral angle O7H6S5C2 does not hold the suitable symmetry. Conversely, complete relaxation of the rest of coordinates but the distances corresponding to the breaking and the forming bonds leads to an energy profile involving two symmetrically equivalent minima ($P = 1$ and $\sigma = 2$). Three dihedral angles, H1C2S5H6, O7H6S5C2, and H8O7H6S5, change along this path. From the maximum energy points of that profile a direct location (with the distances H6—S5 and O7—H6 frozen) leads to the two quasi-degenerate second-order saddle points shown in Figure 2.
4. Mode 15 at the transition state structure. This mode consists basically of the rotation of the hydroxyl hydrogen around the O7—H6 bond and, therefore, the dihedral angle O7H6S5C2 has to be frozen. Then, we have done a rigid rotation as a function of the dihedral angle H8O7H6S5 ($P = 1$ and $\sigma = 1$). The maximum energy point of this energy profile determines the energy barrier for the internal rotation. Any attempt to relax the dihedral angle O7H6S5C2 leads to the energy profile corresponding to mode 16. In fact, a transition state optimization (with the H6—S5 and O7—H6 distances frozen) starting at the maximum (mentioned above) of the H8O7H6S5 internal rotation actually leads to one of the structures in Figure 2.

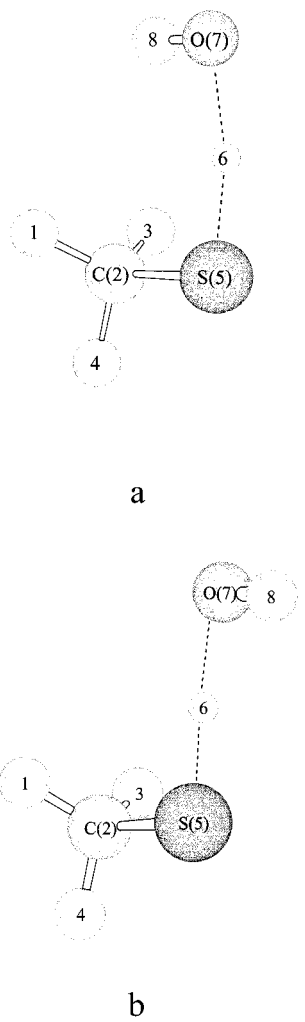

Figure 2. Two quasi-degenerate second-order saddle points corresponding to the internal rotation mode 16 at the transition state structure. The dihedral angle O7H6S5C2 is 0.1° or 180° for (a) and (b), respectively.

Table 2. Moments of Inertia,[a] Energy Barriers,[b] and Estimated Vibrational Harmonic Frequencies[c] for the Three Internal Rotation Modes at the Transition State Structure.

Mode i	I	W	$\bar{\nu}$
17	2.0419×10^4	0.85	119.9
16	2.0344×10^4	2.31	132.0
15	5.6238×10^3	5.66	196.5

[a]In a.u.
[b]In kcal/mol.
[c]In cm^{-1}.

Table 2 exhibits the parameters needed to calculate the hindered rotor partition functions according to the CW scheme[19] for the three internal rotation modes at the transition state structure. The corresponding parameters for the unique internal rotation mode at the methanethiol are 7.3615×10^3 a.u., 1.48 kcal/mol and 263.4 cm^{-1} for the moment of inertia, the energy barrier and the estimated vibrational harmonic frequency, respectively. It has to be noted that the internal rotation of methyl group around the C2—S5 bond at the transition state structure is quite easier than at the methanethiol.

Table 3. Harmonic Vibrational Partition Functions and Their Global Contribution to the Rate Constant.

$T(K)$	$q^R_{CH_3}$	$q^{\ddagger}_{CH_3}$	$q^{\ddagger}_{OH}$	$q^{\ddagger}_{H}$	Global contribution
100	0.1636	0.6433	0.4789	0.2327	0.4382
150	0.3218	1.011	0.7737	0.4224	1.027
200	0.4750	1.370	1.059	0.6041	1.844
250	0.6232	1.725	1.341	0.7805	2.897
300	0.7681	2.079	1.619	0.9538	4.180
400	1.052	2.783	2.174	1.295	7.448
600	1.609	4.187	3.276	1.968	16.78
800	2.159	5.589	4.376	2.636	29.86
1000	2.708	6.989	5.474	3.302	46.65
1500	4.074	10.49	8.218	4.964	105.0
3000	8.164	20.89	16.44	9.941	420.0
5000	13.61	34.97	27.41	16.57	1167.

The harmonic vibrational partition functions as a function of the temperature for the unique internal rotation mode of methanethiol and for the three modes of the transition state structure are presented in Table 3. These partition functions arise from the vibrational harmonic frequencies directly obtained through the diagonalization of the Hessian matrices (note that q^{HO} in eq. (5) is only an estimate of the actual harmonic vibrational partition function). The global contribution of these internal rotation modes (the product of the three transition state partition functions divided by the methanethiol partition function), treated as harmonic, to the rate constant is given in the last column. The corresponding hindered rotor partition functions and their global contribution to the rate constant are presented in Table 4. The hindered rotor partition functions for the internal rotation mode of methanethiol and for modes 17 and 16 of the transition state structure turn out always to be somewhat smaller than their harmonic counterparts, the differences between them not being very significant up to high temperatures are reached. Conversely, the hindered rotor partition functions for mode 15 appear to be slightly bigger than the corresponding harmonic ones (except at 5000 K). This is probably due to the fact that they have been obtained using the estimated vibrational harmonic frequencies [see eq. (6)] in the interpolation. Anyway, for this mode no important difference between the hindered rotor and the harmonic partition functions appear at any temperature. The results on Tables 3 and 4 can be understood realizing that, according to the eq. (5) and, because $P = 1$ for all the studied modes, the ratio q^{HR}/q^{HO} depends on the hyperbolic tangent of a quantity proportional to the quotient

$$\frac{I^{1/2}\bar{\nu}}{\sigma T^{1/2}}$$

for each internal rotation mode. So, the smaller that quotient, the lower the ratio q^{HR}/q^{HO}. Finally, comparing the global contribution of the internal rotation modes, it can be seen that using the hindered rotor partition functions the rate constant is reduced by a factor of, for instance, 0.87, 0.85, 0.75 or 0.42 at 200, 300, 1000, or 5000 K, respectively (see last column in Table 4).

Table 4. Hindered Rotor Partition Functions and Their Global Contribution to the Rate Constant.

$T(K)$	$q^R_{CH_3}$	$q^{\ddagger}_{CH_3}$	$q^{\ddagger}_{OH}$	$q^{\ddagger}_{H}$	Global contribution	(HR/HO)[a]
100	0.1539	0.5128	0.4549	0.2585	0.3918	0.8941
150	0.3072	0.8191	0.7392	0.4594	0.9055	0.8817
200	0.4555	1.112	1.014	0.6516	1.612	0.8742
250	0.5980	1.393	1.284	0.8387	2.509	0.8661
300	0.7359	1.666	1.550	1.023	3.589	0.8586
400	1.001	2.186	2.076	1.385	6.280	0.8432
600	1.498	3.135	3.100	2.101	13.63	0.8123
800	1.959	3.983	4.086	2.807	23.32	0.7810
1000	2.388	4.751	5.031	3.507	35.11	0.7526
1500	3.347	6.414	7.224	5.217	72.23	0.6879
3000	5.599	10.16	12.66	9.955	228.7	0.5445
5000	7.835	13.81	18.25	15.40	495.4	0.4245

[a]Ratio of hindered rotor to harmonic oscillator global contributions.

We have to underline that the reaction in eq. (3) provides a special case in which the use of the hindered rotor treatment could be supposed to be highly recommended because the transition state structure includes three low-frequency internal rotation modes. However, our results show that at room temperature or below, that treatment is not critical to obtain accurate values of the rate constant. In this case it is true that the hindered rotor partition functions decrease the calculated rate constants, but the improvement is rather modest in comparison with other much more important sources of error that affect the calculation of the reaction rate constants. Then, from the results of this article, we can conclude that torsional anharmonicity will generally be small for cases with no torsion frequencies below about 100 cm^{-1} and no torsion barriers below about 0.8 kcal/mol, independently on the number of low-frequency internal rotation modes. Additional theoretical work is now in progress in our laboratory to test the effect of torsional anharmonicity on the rate constants of chemical reactions including torsion frequencies or torsion energy barriers below the above mentioned values.

Acknowledgement

The use of the computational facilities of the CESCA is gratefully acknowledged.

References

1. Truhlar, D. G.; Garrett, B. C.; Klippenstein, S. J. J Phys Chem 1996, 100, 12771.
2. Glasstone, S.; Laidler, K. J.; Eyring, H. The Theory of Rate Processes; McGraw-Hill: New York, 1941.
3. Steinfeld, J. I.; Francisco, J. S.; Hase, W. L. Chemical Kinetics and Dynamics; Prentice Hall: Englewood Cliffs, NJ, 1999.
4. Mc Quarrie, D. A. Statistical Thermodynamics; University Science Books: Mill Valley, CA, 1985.
5. Pacey, P. D. J Chem Phys 1982, 77, 3540.
6. Truong, T. N.; Truhlar, D. G. J Chem Phys 1990, 93, 1761.
7. Liu, Y. P.; Lu, D.-h.; González–Lafont, A.; Truhlar, D. G.; Garrett, B. C. J Am Chem Soc 1993, 115, 7806.
8. Melissas, V. S.; Truhlar, D. G. J Phys Chem 1994, 98, 875.
9. McClurg, R. B.; Flagan, R. C. J Chem Phys 1997, 106, 6675.
10. Schwartz, M.; Marshall, P.; Berry, R. J.; Ehlers, C. J.; Petersson, G. A. J Phys Chem A 1998, 102, 10074.
11. Masgrau, L.; González–Lafont, A.; Lluch, J. M. J Chem Phys 2001, 114, 2154.
12. Masgrau, L.; González–Lafont, A.; Lluch, J. M. J Chem Phys 2001, 115, 4515.
13. Masgrau, L.; González–Lafont, A.; Lluch, J. M. Theo Chem Acc 2002, 108, 38.
14. Lorant, F.; Behar, F.; Goddard, W. A., III; Tang, Y. J Phys Chem A 2001, 105, 7896.
15. Ayala, P. Y.; Schlegel, H. B. J Chem Phys 1998, 108, 2314.
16. Peng, C.; Ayala, P. Y.; Schlegel, H. B.; Frisch, M. J. J Comput Chem 1996, 17, 49.
17. Nguyen, K. A.; Jackels, C. F.; Truhlar, D. G. J Chem Phys 1996, 104, 6491.
18. Truhlar, D. G. J Comput Chem 1991, 12, 266.
19. Chuang, Y.-Y.; Truhlar, D. G. J Chem Phys 2000, 112, 1221.
20. Atkinson, R.; Perry, R. A.; Pitts, J. N., Jr. J Chem Phys 1977, 66, 1578.
21. Wine, P. H.; Kreutter, N. M.; Gump, C. A.; Ravishankara, A. R. J Phys Chem 1981, 85, 2660.
22. Hatakemaya, S.; Akimoto, H. J Phys Chem 1983, 87, 2387.
23. Lee, J. H.; Tang, I. N. J Chem Phys 1983, 78, 6646.
24. Cox, R. A.; Sheppard, D. Nature 1980, 284, 330.
25. Hynes, A. J.; Wine, P. H. J Phys Chem 1987, 91, 3672.
26. Tindall, G. S.; Ravishankara, A. R. J Phys Chem 1989, 93, 4707.
27. Butkovskaya, N. I.; Setser, D. W. J Phys Chem A 1998, 102, 6395.
28. Butkovskaya, N. I.; Setser, D. W. J Phys Chem A 1999, 103, 6921.
29. Hehre, W. J.; Radom, L.; Schleyer, P. v. R.; Pople, J. A. Ab Initio Molecular Orbital Theory; Wiley: New York, 1986.
30. Dunning, T. H. J Chem Phys 1989, 90, 1007.
31. Schlegel, H. B. Geometry Optimization on Potential Energy Surfaces; World Scientific Publishing: Singapore, 1994.
32. Frisch, M. J.; Trucks, G. W.; Schlegel, H. B.; Scuseria, G. E.; Robb, M. A.; Cheeseman, J. R.; Zakrzewski, V. G.; Montgomery, J. A.; Stratmann, R. E.; Burant, J. C.; Dapprich, S.; Millam, J. M.; Daniels, A. D.; Kudin, K. N.; Strain, M. C.; Farkas, O.; Tomasi, J.; Barone, V.; Cossi, M.; Cammi, R.; Mennucci, B.; Pomelli, C.; Adamo, C.; Clifford, S.; Ochterski, J.; Petersson, G. A.; Ayala, P. Y.; Cui, Q.; Morokuma, K.; Malick, D. K.; Rabuck, A. D.; Raghavachari, K.; Foresman, J. B.; Cioslowski, J.; Ortiz, J. V.; Stefanov, B. B.; Liu, G.; Liashenko, A.; Piskorz, P.; Kamaromi, I.; Gomperts, R.; Martin, R. L.; Fox, D. J.; Keith, T.; Al-Laham, M. A.; Peng, C. Y.; Nanayakkara, A.; Gonzalez, C.; Challacombe, M.; Gill, P. M. W.; Johnson, B. G.; Chen, W.; Wong, M. W.; Andres, J. L.; Head–Gordon, M.; Replogle, E. S.; Pople, J. A. Gaussian 98; Gaussian Inc.: Pittsburgh, PA, 1998.
33. Corchado, J. C.; Chuang, Y.-Y.; Fast, P. L.; Villà, J.; Hu, W.-P.; Liu, Y.-P.; Lynch, G. C.; Nguyen, K. A.; Jackels, C. F.; Melissas, V.; Lynch, B. J.; Rossi, I.; Coitiño, E. L.; Fernández–Ramos, A.; Pu, J.; Steckler, R.; Garrett, B. C.; Isaacson, A. D.; Truhlar, D. G. Polyrate 8.7; University of Minnesota, 2001 (http://comp.chem.umn.edu/polyrate).
34. Pitzer, K. S.; Gwin, W. D. J Chem Phys 1942, 10, 428.
35. Pitzer, K. S. J Chem Phys 1946, 14, 239.
36. Kilpatrick, J. E.; Pitzer, K. S. J Chem Phys 1949, 17, 1064.
37. Ozkabak, A. G.; Goodman, L. J Chem Phys 1992, 96, 5958.
38. Wiberg, K. B. Encyclopedia of Computational Chemistry; Wiley: New York, 1998; p 2518.
39. Goodman, L.; Pophristic, V. Encyclopedia of Computational Chemistry; Wiley: New York, 1998; p 2525.